REVIEW OF RESEARCH
IMPACT FACTOR : 5.7631(UIF) UGC APPROVED JOURNAL NO. 48514 ISSN: 2249-894X
VOLUME - 8 | ISSUE - 6 | MARCH - 2019

SYNTHESIS AND INVESTIGATIONS ON STRUCTURAL, ELASTIC AND MAGNETIC PROPERTIES OF NI-CD FERRITES

R. M. More[1] and N. D. Chaudhari[2]
[1]Department of Physics, D. B. J. College, Chiplun, Dist. Ratnagiri, MS.
[2]Department of Physics, Pratishthan Mahavidyalaya, Paithan, Dist. Aurangabad, MS.

ABSTRACT :

Various compositions of $Cd_xNi_{1-x}Fe_2O_4$ ferrites with x = 0.0, 0.2, 0.4, 0.6, 0.8 and 1.0 were synthesized by using oxalate co-precipitation. The synthesized sintered powder was characterized by X-ray diffraction technique and it confirms the formation of cubic spinel structure. Lattice parameter is found to increase with increase in cadmium content obeying Vegard's law. The x-ray density and actual density value shows increasing trend with increase in Cd^{2+}content. The structural parameters such as tetrahedral, octahedral bond lengths, cation-cation and cation-anion distances, bond angles, hopping lengths, tetrahedral edge and shared, unshared octahedral edge were calculated and found to increase with increasing Cd^{2+} content. This could be related to larger Cd^{2+} ions at tetrahedral site as compared to Ni^{2+} ions at octahedral site. IR spectra of cadmium substituted nickel ferrites are found to exhibit two major bands in the range 400-700 cm^{-1}. The high frequency band υ_1 is observed in the range 544-588 cm^{-1} and lower frequency band υ_2 in the range 418-455 cm^{-1}. Force constants for tetrahedral and octahedral site were calculated using IR data and cation distribution of present ferrite compositions. The elastic modili such as Young's Modulus, Bulk Modulus, Shear Modulus, and Longitudinal Modulus, Poisson's ratio, longitudinal velocity, Transverse velocity, mean velocity and Debye temperature were determined. All these elastic moduli increase with increase in Cd^{2+} content. Saturation magnetization (Ms) values are found to be increasing with increase in Cd content up to x = 0.4, obeying Neel's model and decreasing thereafter suggesting the existence of non-collinear spin interaction.

KEYWORDS : *Ni-Cd ferrites, X-ray diffraction, Infra-red spectroscopy, Saturation* ***Magnetization***

INTRODUCTION

Spinel ferrites are very important materials because of their interesting structural, electrical and magnetic properties. They have potential applications in different technological fields such as Ferro-fluids, magnetic resonance imaging (MRI), magnetic drug delivery, memory devices, magnetic high density storage devices, sensors, satellite communication, magnetic recording media, cancer treatment, pigments, etc [1-10].

In spinel ferrites, the metallic cations occupy the tetrahedral (A) site and octahedral (B) site in the unit cell. Nickel ferrite has inverse spinel structure in which entire Ni^{2+} ions and half of Fe^{3+} ions occupy octahedral (B) site and remaining Fe^{3+} ions reside in tetrahedral (A) site whereas Cadmium ferrite has a normal spinel structure. Cd^{2+} is a non-magnetic divalent ion occupying tetrahedral site and shows similar behavior as that of Zn^{2+} substitution [11]. It is known that the distribution of cations among the tetrahedral and octahedral site have significant effect on the structural, electrical and magnetic properties [12-13].
Technologically point of view mixed Cadmium ferrites are known to be more important ferrite material because of their high resistivity, high permeability and low magnetic losses which makes them suitable for

electrical switching applications [14]. The properties of these ferrite materials strongly depend on their chemical composition, substitution and preparatory techniques / conditions [15]. A variety of methods have been developed and used for the preparation of ferrite material such as ceramic, co-precipitation, sol-gel, hydrothermal, citrate precursor, oxalate precursors [16-20]. Among all these various methods, co-precipitation is most convenient method for the preparation because of its simplicity, composition flexibility and homogeneity [21]. Several researchers [22-25] thoroughly studied various properties of Ni-Cd ferrites but a very little work has been discussed on their structural parameters and elastic modulli as compared to their electric and magnetic properties. In present work, the investigation of compositional variation of structural parameters, elastic moduli and magnetization of Ni-Cd ferrites synthesized using co-precipitation route is reported.

EXPERIMENTAL:

Various compositions of stoichiometric series $Cd_xNi_{1-x}Fe_2O_4$ (x = 0.0, 0.2, 0. 4, 0.6, 0.8, 1.0) were synthesized by oxalate co-precipitation method using sulphates. The high purity AR grade nickel sulphate, cadmium sulphate, and ferrous sulphate were weighed carefully to have proper stoichiometric proportion required in the final product. The mixed solution of required compounds was prepared in double distilled water. Precipitate was formed by adding the solution of AR grade ammonium oxalate in the solution of sulphates. The pH of the solution was kept about 4.7.

Sulphates present in the precipitate were thoroughly washed with distilled water and filtered. The absence of sulphates in the filtrate was confirmed with barium chloride test. The precipitate was dried presintered at 600 ^{0}C for one hour in air. The presintered powder was milled in an agate mortar with AR grade acetone as a base. The samples were finally sintered at 1000 ^{0}C for two hours in air.

The synthesized ferrite compositions were characterized by using X-ray powder diffraction. The computerized X-ray diffractometer, model Philips PW1710 was used. The wavelengths of radiations used were λ_1 = 2.2897 Å and λ_2 = 2.29361 Å. The IR spectra of the composition $Cd_xNi_{1-x}Fe_2O_4$ system were obtained in the range from 350 cm^{-1} to 800 cm^{-1}, using Perkin-Elmer Spectrophotometer, model 783, using KBr as a solvent.

RESULTS AND DISCUSSION:

A] X-RAY DIFFRACTION:

The X-ray diffractograms of polycrystalline powdered compositions of $Cd_xNi_{1-x}Fe_2O_4$, (for x = 0.0, 0.2, 0.4, 0.6, 0.8 and 1.0) are presented in Fig. 1. The diffraction maxima have been indexed for spinel structure. The reflections observed are 111, 220, 311, 222, 400, 331, 422, 511, 440 and 533. These reflections correspond to the allowed values of reflections for cubic spinel structure. The X-ray diffractograms do not point out the occurrence of any unwanted phase with different Ni-Cd ferrites confirming the single-phase spinel formation.

The experimental lattice parameter ($a_{exp.}$) of sintered samples are calculated from the relation

$$a_{exp.} = d_{hkl}[h^2+k^2+l^2]^{1/2} \quad \text{--------- [1]}$$

It is also known that there is a relation between ionic radii of A and B sub lattices and lattice parameter. Then the theoretical lattice parameter $a_{th.}$of investigated compositions are calculated from the equation [26]

$$a_{th.} = \frac{8}{3}\sqrt{3}\left[(rA + Ro) + \sqrt{3}(rB + Ro)\right] \quad \text{---------- [2]}$$

Where R_o is radius of oxygen ion= 1.38Å, r_A, r_B are ionic radii of tetrahedral [A] and octahedral [B] site.

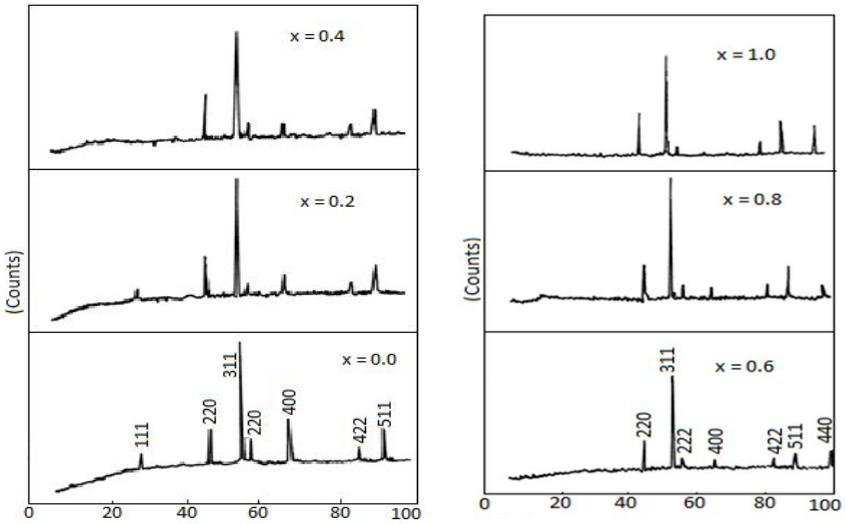

Fig. 1: XRD patterns for $Cd_xNi_{1-x}Fe_2O_4$ ferrites

The values of lattice parameter are presented in Table 1. These values show good agreement with the values reported for $NiFe_2O_4$ [27], and $CdFe_2O_4$ [28]. It is observed that the lattice parameter increases with increase of cadmium content obeying Vegard's law. This is due to large ionic radius of Cd^{2+} (0.99 A^0) [29], as compared to that of Ni^{2+} (0.74A^0); which when substituted resides on A site and displaces proportional amount of Fe^{3+} ions (ionic radius 0.67 A^0) on B site.The effect of Cd^{2+} substitution on X-ray density, actual density and porosity is shown in Table 1. The X- ray density was calculated using the relation [30].

$$\rho_x = \frac{8M}{N_A a^3} \text{--------- [3]}$$

It is known that X-ray density depends on the value of lattice parameter. It is observed that the x-ray density and actual density value shows increasing trend with increase in Cd^{2+}content. This is due to the difference in ionic radii between Ni and Cd. It is also observed that the magnitudes of X-ray densities are higher than that of actual densities. This may be due to the existence of pores occurring in sample preparation and during sintering process.

Table 1: Data on lattice parameter ($a_{exp.}$&$a_{th.}$), Oxygen parameter (u), X-ray density (ρ_x), actual density (ρ_a) and % porosity for present ferrite system

x	a_{expt} (Å)	$a_{theo.}$(Å)	u	ρ_x(gm/cc)	ρ_a(gm/cc)	Porosity %
0.00	8.32	8.32	0.375	5.41	4.53	16.26
0.20	8.39	8.39	0.375	5.51	4.69	14.88
0.40	8.43	8.43	0.375	5.67	4.94	12.87
0.60	8.53	8.53	0.375	5.71	5.05	11.56
0.80	8.60	8.60	0.375	5.79	5.18	10.53
1.00	8.70	8.70	0.375	5.81	5.22	10.16

The oxygen positional parameter values (u) are determined using the values of a –lattice parameter, radius of oxygen ions R = 1.38Å and r_A – tetrahedral ionic radii using a relation given by [31]

$$u = [(rA + Ro)\frac{1}{\sqrt{3}a} + \frac{1}{4}] \quad \text{--------- [4]}$$

Using the experimental values of lattice parameter and oxygen parameter of each composition, different structural parameters such as bond length [d_{AX}, d_{BX}], site radii [r_A, r_B], tetrahedral edge [d_{XX}], shared and unshared octahedral edges [d'_{XX}, d''_{XX}], hopping length [L_A, L_B] are determined using the relations [32] and summarized in Table 2.

$$d_{AX} = a\sqrt{3}\left(u - \frac{1}{4}\right) \quad \text{--------- [5]}$$

$$d_{BX} = a\sqrt{3u^2 - \frac{11}{4}u + \frac{43}{64}} \quad \text{--------- [6]}$$

$$d_{XX} = a\sqrt{2}\left(2u - \frac{1}{2}\right) \quad \text{---------- [7]}$$

$$d'_{XX} = a\sqrt{2}\,(1 - 2u) \quad \text{---------- [8]}$$

$$d''_{XX} = a\sqrt{4u^2 - 3u + \frac{11}{16}} \quad \text{---------- [9].}$$

$$L_A = a\frac{\sqrt{3}}{4} \quad \text{---------- [10]}$$

$$L_B = a\frac{\sqrt{2}}{4} \quad \text{---------- [11]}$$

Table 2: Data on hopping lengths (L_A& L_B), bond length (d_{AX}, d_{BX}), site radii (r_A, r_B), tetrahedral edge (d_{XX}), shared and unshared octahedral edges (d'_{XX}, d''_{XX}) for present ferrite system.

x	d_{AX}	d_{BX}	r_A	r_B	d_{XX}	d'_{XX}	d''_{XX}	L_A	L_B
0.00	1.8013	2.0800	0.4213	0.7000	2.9416	2.9416	2.9416	3.6027	2.9416
0.20	1.8165	2.0975	0.4365	0.7175	2.9663	2.9663	2.9663	3.633	2.9663
0.40	1.8252	2.1075	0.4451	0.7275	2.9804	2.9805	2.9805	3.6503	2.9805
0.60	1.8468	2.1325	0.4668	0.7525	3.0158	3.0158	3.0158	3.6936	3.0158
0.80	1.8619	2.1500	0.4820	0.7700	3.0405	3.0406	3.0406	3.7239	3.0406
1.00	1.8836	2.1750	0.5036	0.795	3.0759	3.0759	3.0759	3.7672	3.0759

The site radii (r_A, r_B) are determined using the values d_{AX}, d_{BX} taking 1.38 Å as a radius of oxygen ion. It is observed that tetrahedral bond length (d_{AX}), octahedral bond length (d_{BX}), tetrahedral edge (d_{XX}) and shared and unshared octahedral edge (d'_{XX}, d''_{XX}), hopping length (L_A and L_B) increases with increasing Cd^{2+} content. This could be related to larger Cd^{2+} ions at tetrahedral site as compared to Ni^{2+} ions at octahedral site. Similar observations have been observed by V. M. Khot et al [32] for Mn substituted Mg ferrites.

The cation-cation (Me-Me) and cation-anion (Me-O) bond distances are determined using a following relation [33]

Cation-cation distances (Me-Me)

$$b = \left(\frac{a}{4}\right)\sqrt{2} - - \ [12a] \qquad c = \left(\frac{a}{8}\right)\sqrt{11} \quad \text{----- [12b]}$$

$$d = \left(\frac{a}{4}\right)\sqrt{3} - -[12c] \qquad e = \left(\frac{3a}{8}\right)\sqrt{3} \quad \text{----- [12d]}$$

$$f = \left(\frac{a}{4}\right)\sqrt{6} \quad \text{---- [12e]}$$

Cation-anion distances (Me-O)

$$p = a\left[\left(\frac{5}{8}\right) - u\right] - -[13a] \qquad q = a\left[u - \left(\frac{1}{4}\right)\sqrt{3}\right] \quad \text{----- [13b]}$$

$$r = a\left[u - \left(\frac{1}{4}\right)\sqrt{11}\right] - [13c] \qquad s = a\left[\left(\frac{u}{3}\right) + \left(\frac{1}{8}\right)\right]\sqrt{3} \quad \text{---- [13d]}$$

Table 3: Data on the values of cation-cation (Me-Me) and cation-anion bond (Me-O) distances for present ferrite system

x	cation-cation bond distances					cation-anion bond distances			
	b	c	d	e	f	p	q	r	s
0.00	2.9416	3.4493	3.6027	5.404	5.0949	2.0800	1.8013	3.4493	3.6027
0.20	2.9663	3.4783	3.633	5.4495	5.1378	2.0975	1.8165	3.4783	3.633
0.40	2.9805	3.4949	3.6503	5.4754	5.1623	2.1075	1.8252	3.4949	3.6503
0.60	3.0158	3.5364	3.6936	5.5404	5.2235	2.1325	1.8468	3.5364	3.6936
0.80	3.0406	3.5654	3.7239	5.5858	5.2664	2.1500	1.8619	3.5654	3.7239
1.00	3.0759	3.6068	3.7672	5.5608	5.3276	2.1750	1.8836	3.6068	3.7672

The cation-cation distances (Me-Me) and cation-anion distances (Me-O) are tabulated in Table 3. It is observed that the cation-cation distances (Me-Me) and cation-anion distances (Me-O) increases with increase in Cd^{2+} ions in the system. This may be again related to the ionic radius of Ni^{2+} and Cd^{2+} ions

involved in the system and variation of lattice constant. B.B.V.S. Vara Prasad et al [33] have been observed an increase in cation-cation and cation-anion distances in Mg^{2+} substituted Ni-Zn ferrites and attributed it to the Mg incorporation into octahedral site by replacing Ni in octahedral site which resulting in the expansion of lattice and little displacement of oxygen ions. The angles between these interionic distances (bond angles) were determined using the simple trigonometric formulae [33].

$$\theta_1 = cos^{-1}\left[\frac{(p^2+q^2-c^2)}{2pq}\right] \text{ ------- [13a]}$$

$$\theta_2 = cos^{-1}\left[\frac{(p^2+r^2-c^2)}{2pr}\right] \text{ ------- [13b]}$$

$$\theta_3 = cos^{-1}\left[\frac{(2p^2-b^2)}{2p^2}\right] \text{ ------- [13c]}$$

$$\theta_4 = cos^{-1}\left[\frac{(p^2+s^2-f^2)}{2ps}\right] \text{ ------- [13d]}$$

$$\theta_5 = cos^{-1}\left[\frac{(r^2+q^2-d^2)}{2rq}\right] \text{ ------- [13e]}$$

The bond angles are presented in Table 04. It is observed that the bond angles remains constant with increase in Cd^{2+} content. A slight deviation is observed from ideal bond angles compared to reported values.

Table 4: Data on the values of bond angles (θ_1, θ_2, θ_3, θ_4, θ_5) in degrees for present ferrite system.

x	θ_1	θ_2	θ_3	θ_4	θ_5
0.00	125.25	154.74	89.98	125.25	79.96
0.20	125.25	154.74	89.98	125.25	79.96
0.40	125.25	154.74	89.98	125.25	79.96
0.60	125.25	154.74	89.98	125.25	79.96
0.80	125.25	154.74	89.98	125.25	79.96
1.00	125.25	154.74	89.98	125.25	79.96

B] IR SPECTROSCOPY:

Infrared absorption spectrophotometry is the important tool to describe the various ordering problems [34]. It is a nondestructive and rapid method of characterization and provides the qualitative analysis regarding the structure of functional groups and their linkages. From IR spectral analysis, one can extract the information regarding formation of spinel structure, nature of metal oxygen bonds, cation distribution, force constant, electronic structure etc. According to Waldron [35] the vibration of unit cell of cubic spinel structure can be divided in tetrahedral A site and octahedral B site. The high frequency absorption band υ_1 is caused by the stretching vibration of tetrahedral metal-oxygen bond and low frequency absorption band υ_2 is caused by metal-oxygen vibration in octahedral sites and attributed the absorption band ν_1 to the intrinsic vibration of tetrahedral groups corresponding to the highest restoring force and band ν_2 to octahedral groups which are bond bending vibrations.The absorption band, from which the structural information can be explored, is found to be dependent on atomic mass, cationic radius, cation - anion bond distance, method of preparation, chemical compositions etc [34,36].

The Infrared spectra for $Cd_xNi_{1-x}Fe_2O_4$ ferrites are shown in Fig. 2. It is observed that the IR spectra of cadmium substituted nickel ferrites are found to exhibit two major bands in the range 400-700 cm^{-1}. The high frequency band υ_1 is observed in the range 544-588 cm^{-1} and lower frequency band υ_2 in the range 418-455 cm^{-1} and confirms the formation of spinel ferrite structure. The values of $\upsilon_1$and υ_2 are given in Table 5. It is observed that high frequency band position υ_1 shift towards higher values whereas low frequency band $\upsilon_2$initially increase thereafter shift towards lower values with increasing Cd^{2+} content. It is known that Cd^{2+} ions occupied tetrahedral A site in cation distribution and have larger ionic radius, higher atomic weight as compared to nickel ion in octahedral site which affect the band positions.

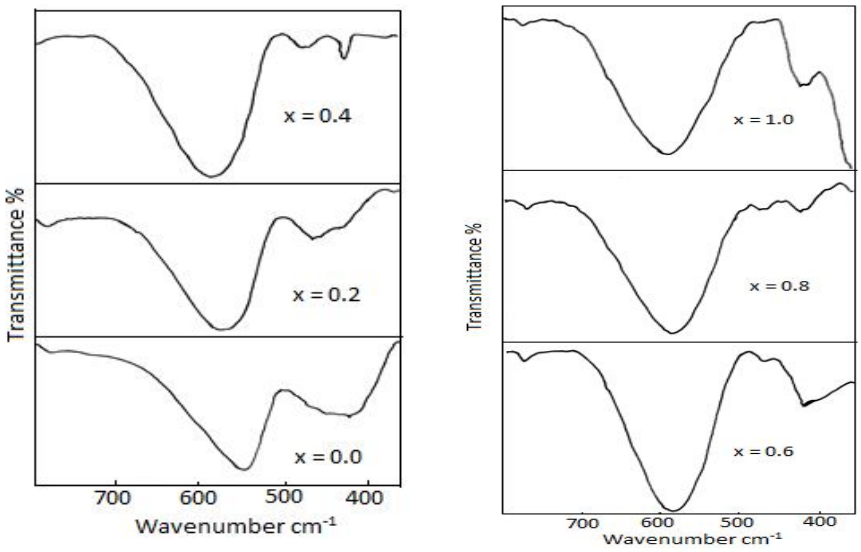

Fig. 2: IR spectra for $Cd_xNi_{1-x}Fe_2O_4$ ferrites

The difference in the positions of high frequency band and low frequency band is due to the difference in the Fe^{3+}-O^{2-} distances for the tetrahedral and octahedral complexes. The Fe-O distance of tetrahedral (A) site is smaller than that of octahedral (B) site [37] which can be explained by the stronger covalent bonding of Fe^{3+} at a site than B site.

Using the values of high frequency and low frequency bands, the force constants corresponding to the tetrahedral and octahedral sites are determined by using the formulae [38] and tabulated in the Table 5.

$$K_t = 7.62 \times M_1 \times \upsilon_1^2 \times 10^{-7} \text{ N/m} \quad \text{--------- [14]}$$

$$K_0 = 10.62 \times \frac{M_2}{2} \times \upsilon_2^2 \times 10^{-7} \text{ N/m} \quad \text{--------- [15]}$$

Where K_o = force constant of octahedral (B) site

K_t = force constant of tetrahedral (A) site

M_1 = molecular weight of tetrahedral (A) site

M_2 = molecular weight of octahedral (B) site

v_1 = corresponding frequency band on tetrahedral (A) site

v_2 = corresponding frequency band on octahedral (B) site

The force constant as a function of Cd^{2+} content have been determined using the cation distribution $(Cd_xFe_{1-x})^A [Ni_{1-x}Fe_{1-x}]^B O_4$. It is seen that the force constant K_t increases as Cd^{2+} content increases whereas K_0 decreases with increasing Cd^{2+} content. This variation in force constants may be due to the difference of ionic radii of Cd^{2+}, Ni^{2+} and Fe^{3+} ions.

Debye temperature was estimated by using a relation given by [35, 39] and are of great importance to determine the heat conduction mechanism of the ferrites.

$$\theta_1 = 1.438 \times \upsilon_{av.} \quad \text{------- [16]}$$

Where $\upsilon_{av} = \left(\frac{\upsilon_1 + \upsilon_2}{2}\right)$

The Debye temperatures obtained from above relation arelies in the range (692-723) K and found to increase with increase in Cd^{2+} content.

The longitudinal wave velocity (V_L) and transverse wave velocity (V_T) are estimated as follows [40] and listed in Table 5.

$$V_L = \left(\frac{C_{11}}{\rho_a}\right)^{1/2} \quad \text{-------- [17]} \qquad V_t = \frac{V_L}{\sqrt{3}} \quad \text{--------- [18]}$$

The average force constant k_{av} is the product of stiffness constant (C_{111} = L, longitudinal modulus) and lattice parameter (a). ρ_a is the density. The values of longitudinal and transverse wave velocities are

found to increase with increase in Cd^{2+} content. The values of longitudinal wave velocity are greater than those of thetransverse wave velocity. Lakani et al [41] explained this behavior as in case of transverse wave velocity, the particles in the medium vibrate perpendicular to the direction of propagation of wave motion, hence it required a large energy to make the neighboring particles vibrate accordingly resulting in the reduction in the energy of wave and hence the velocity of transverse wave is nearly half of the velocity of longitudinal wave.

Table 5: Data on vibrational bands (v_1 and v_2), force constants (K_t and K_0), longitudinal wave velocity (V_L), Transverse wave velocity (V_T) and Mean wave velocity (V_m)for present ferrite system.

x	v_1 (cm^{-1})	v_2 (cm^{-1})	K_t (N/m)	K_0 (N/m)	V_L (m/s)	V_T (m/s)	V_M (m/s)
0.00	544	418	125.93	106.26	5550	3204	3557
0.20	567	455	164.52	125.28	6068	3503	3889
0.40	575	421	197.7	106.72	6045	3490	3875
0.60	583	420	232.54	105.68	6265	3617	4016
0.80	587	418	265.44	104.15	6440	3718	4128
1.00	588	418	296.15	103.62	6634	3830	4252

The different elastic moduli for $Cd_xNi_{1-x}Fe_2O_4$were determined using the following relation [42].

$$\text{Shear Modulus (G)} = \rho \times (V_t)^2 \text{ ---------- [19]}$$

$$\text{Bulk modulus (B)} = L - \left(\frac{4}{3}\right) G \text{ ---------- [20]}$$

$$\text{Young's Modulus (E)} = (1+\sigma)2G \text{ ---------- [21]}$$

$$\text{Poisson's ratio } (\sigma) = \frac{3B-2G}{6B+2G} \text{ ---------- [22]}$$

$$\text{Mean wave velocity } (V_m) = \left[\frac{1}{3}\left(\frac{1}{{V_L}^3} + \frac{2}{{V_t}^3}\right)\right]^{-1/3} \text{ ---------- [23]}$$

The values of these elastic moduli are tabulated in Table 6. It is observed that all these elastic moduli increases with increase in Cd^{2+} content. That may be due to strengthening of inter atomic bonding between various atoms of spinel lattice. Similar observations have been made by A. Maqsood et. al [43] for Ni-Cd nanoferrites.

Table 6: Data on Longitudinal modulus (L), Shear modulus (G), Bulk modulus (B), Young modulus (E), Poisson's ratio (σ), elastic moduli corrected to zero porosity (E_0, G_0, B_0, L_0, σ_0)

x	L(GPa)	G(GPa)	B (GPa)	E (GPa)	E_0 (GPa)	G_0 (GPa)	B_0 (GPa)	L_0 (GPa)	σ	σ_0
0.00	139.54	46.51	77.52	116.28	172.58	68.08	123.68	214.45	0.25	0.27
0.20	172.71	57.57	95.94	143.92	205.15	81.22	144.25	252.53	0.25	0.26
0.40	180.56	60.19	100.31	150.46	202.84	80.45	141.22	248.48	0.25	0.26
0.60	198.25	66.08	110.14	165.21	215.06	85.40	148.85	262.71	0.25	0.26
0.80	214.88	71.63	119.38	179.06	227.03	90.22	156.47	276.76	0.25	0.26
1.00	229.76	76.58	127.64	191.46	240.43	95.57	165.44	292.87	0.25	0.26

As the polycrystalline ferrite materials are porous then the values of elastic constants have been corrected to zero porosity. The elastic moduli corrected to zero porosity are determined using Hasselman and Fulrath formulae [44].

$$\frac{1}{E_0} = \frac{1}{E}\left[1 - \frac{3f(1-\sigma)(9+5\sigma)}{2(7-5\sigma)}\right] \text{ ---------- [24]}$$

$$\sigma_0 = \left[\frac{E_0}{2G_0} - 1\right] \text{ ---------- [25]}$$

$$\frac{1}{G_0} = \frac{1}{G}\left[1 - \frac{15f(1-\sigma)}{(7-5\sigma)}\right] \text{ ---------- [26]}$$

$$L_0 = K_0 + \frac{4}{3}G_0 \text{ ---------- [27]}$$

$$K_0 = \left[\frac{E_0 G_0}{3(3G_0 - E_0)}\right] \text{ ---------- [28]}$$

The elastic moduli corrected to zero porosity are given in Table 6. It is observed that the magnitudes of elastic constants corrected to zero porosity are higher than that of elastic constants which are not corrected to zero porosity.

Debye temperature θ_D was determined using the value of mean wave velocity using the Anderson's relation [45].

$$\text{Debye temperature } (\theta_D) = \frac{h}{K_B}\left(\frac{3\rho q N_A}{4\pi M}\right)^{1/3} V_m \text{ ---------- [29]}$$

Where h =Planck's constant, K_B = Boltzmann constant, N_A = Avogadro's number, M = Molecular weight of the composition, q = Number of atoms in unit formula, ρ = density of the sample

The Debye temperature θ_D obtained from Anderson formula are given in Table 7. It is observed that Debye temperature obtained from Waldron equation is higher than that of Anderson formula. It is also observed that θ_D increases with increase in Cd^{2+} content as similar to the Debye temperature θ_1 obtained from Waldron's equations. Debye temperature represents the temperature at which all the modes of vibrations are excited and increase in it implies the increase in rigidity of ferrite materials.

Table 7: Data on Debye temperatures (θ_D, θ_1), B_0/G_0 ratio for $Cd_xNi_{1-x}Fe_2O_4$ ferrites.

x	θ_D (K)	θ_1 (K)	B_0/G_0
0.00	459	692	1.82
0.20	500	735	1.78
0.40	500	716	1.75
0.60	514	721	1.74
0.80	527	723	1.73
1.00	537	723	1.73

According to the Pugh criteria [46], the ratio of Bulk modulus to Rigidity modulus represents the ductibility/brittleness nature of synthesized material. If this ratio is larger than the critical value 1.75, the material is said to be ductile in nature and if lower than 1.75 then the brittle nature. For the present synthesized ferrite system the ratio is presented in Table 7 and the values are found to be in the range of 1.73 -- 1.82. It is observed that the ratio decreases with increase in Cd^{2+} content in the system.

C] MAGNETIC PROPERTIES:

Magnetic properties include saturation magnetization (Ms), Curie temperature (Tc), susceptibility (χ) and coercive force (Hc) etc. These parameters help to decide the nature of application of ferrites. The value of saturation magnetization depends on the nature of cations and their distribution.

Magnetic hysteresis is a key factor for determining the possible applications of the magnetic materials. The hysteresis properties of ferrites are highly sensitive to their chemical composition, porosity, grain size, crystal structure, cation distribution and microstructure [47]. These properties are also influenced by the conditions of sintering process.

The saturation magnetization measurements of samples of the present system were carried out with the help of high field loop tracer at room temperature. The saturation magnetization Ms (emu / gm), magnetic moment (n_B Bohr Magneton), were determined by using high field loop tracer at room temperature and their values along with Y-K angles are given in Table 8.

Table 8: Saturation magnetization (Ms), magnetic moment (n_B) and Y-K angles for $Cd_xNi_{1-x}Fe_2O_4$ ferrite system.

Cd^{2+} content (x)	Magnetic moment Bohr Magneton	Saturation magnetization Gauss	Y-K angles
0.0	1.97	212.08	17^0 18' 42"
0.2	2.99	307.03	26^0 55' 30"
0.4	3.09	348.12	43^0 23' 22"
0.6	2.20	232.53	61^0 54' 49"
0.8	0.00	0.00	83^0 55' 57"
1.0	0.00	0.00	90^0 0' 0"

From Table 8, it is observed that the saturation magnetization (Ms) values are found to be increasing with increase in Cd content up to x = 0.4, obeying Neel's model for magnetization and decreasing thereafter suggesting the existence of non-collinear spin interaction. Similar behavior has been observed for Ni-Cd ferrites [48].

Similar results were reported by Karche et al [49] for Mg-Cd ferrites. The Ms and n_B increase with Cd^{2+} content up to x = 0.4 and then goes on decreasing. They explained this behavior by suggesting the existence of canted spins. Canting of spins gives rise to Y-K angles, which captures the strength of A-B and B-B super exchange interaction. Hence Neel's two sub-lattice model is applicable for the system up to $x \leq 0.4$ and beyond that, three sub-lattice model is predominant.

The compositional dependence of Ms and n_B with Cd content can be explained on the basis of cation distribution, Neel's theory and Yaffet-Kittle triangular spin concept. The Cd^{2+} has strong preference to A site and Ni^{2+} have preference for B site.

The magnetic moment of Ni^{2+} is of the order of 2.3 μ_B and that of Fe^{3+} ion is 5μ_B. The substitution Cd^{2+} at A site, transfer Fe^{3+} ions from A site to B site, therefore AB interaction goes on decreasing as Cd^{2+} content is increased. The amount of Fe^{3+} is replaced by Cd^{2+} from A site to B site have parallel moments on B site because of strong AB interaction. At lower Cd^{2+} content this trend will continue up to x = 0.4. Therefore saturation magnetization (Ms) and magnetic moment (n_B) goes on increasing. The net magnetization in this region is given by Neel's two sub-lattice model. However, for further increase of Cd^{2+} content the magnetic parameters show decreasing trend. The decrease in magnetization for further Cd^{2+} substitution can be explained by introducing Y-K triangular spin.

Beyond certain limit of cadmium substitution, the B site moment is too weak to affect the B site moments. Therefore B-B interaction becomes strong and decrease of A-B interaction causes the splitting of B sub lattice into two components B1 and B2 which are held at certain non zero angles and resultant of which is considered to be anti-parallel to A site moment. The angle between the components of moments B1, B2 of B site is found to be a function of magnetic ion substitution occupying A site and strength of A-B interaction. As the strength of A-B interaction decreases due to increase of Cd^{2+} content beyond certain percentage, the values of Y-K angles go in increasing thereby reducing net magnetization.

The Y-K angles for the present ferrite system are calculated by using the experimentally observed n_B values and presented in the Table 8. The Y-K angles are found to be increasing with Cd^{2+} content. For $CdFe_2O_4$ it is 90^0. Hence the magnetic moment of two sub-lattice components on B site arranged to give n_B values. The lower values of Y-K angles for lower values of Cd^{2+} content confirm the predominance of Neel two sub-lattice models. In this region the presence of canting angles accounts the deviation from straight line relation of the Cd^{2+} content and observed magnetic moment from their theoretical values. While the higher values of these, beyond certain content of Cd^{2+} confirms the prevalence of Y-K triangular spin model and explains the observed decrease in magnetic moment. The composition for x = 0.8 and 1.0 show paramagnetic behavior.

CONCLUSIONS:

1. Different compositions of $Cd_xNi_{1-x}Fe_2O_4$ with x = 0.0, 0.2, 0.4, 0.6, 0.8, and 1.0 were synthesized using oxalate co-precipitation.
2. Formation of spinel structure was confirmed using X-ray diffraction and IR spectra. The Lattice parameter is found to increase with increase in cadmium content. The structural parameters are found to increase with increasing Cd^{2+} content.
3. IR spectra designate two absorption bands i.e high frequency band υ_1 in the range 544-588 cm^{-1} and lower frequency band υ_2 in the range 418-455 cm^{-1}. The force constants for tetrahedral and octahedral sites were estimated.
4. The elastic moduli were determined using IR data and found to increase with increase in Cd^{2+} content
5. All the elastic moduli are corrected to the zero porosity.

6. The bulk modulus to rigidity modulus ratio is found to decrease with increase in Cd^{2+} content in the system and lies in the range of 1.73 -- 1.82. It leads to conclude that the compositions with x = 0.60-1.0 are somewhat brittle in nature than their counterparts (ductile).
7. Saturation magnetization (Ms) values are found to be increasing with increase in Cd content up to x = 0.4 and decreasing thereafter.

REFERENCES:

1. S. K. Shrivastava, N. S. Gajbhiye: J. Am. Ceram. Soc., 95 (2012) 3678-3682
2. D. Cruickshank: J. euro. Ceram. Soc., 23 (2003) 2721
3. P. Poddar, J. Gass, D. J. Rebar, S. Srinath, H. Srikanth, S. A. Morrison, E. E. Carpenter: J. Magn. Magn.Mater., 307 (2006) 227
4. M. A. Gabal: J. Phys. Chem., 64 (2003) 1375-1385
5. M. Damnjanovic, G. Stojanovic, V. Desnica: IEEE Trans. Magn., 42 (2006) 270
6. M. P. Pileni: Adv. Funct. Mater., 11(5) (2001) 323-336
7. M. A. Gabal, Y. m. Al Angari: Mater. Chem. Phys.,118 (2009) 153-160
8. P. Pulisova, J. Kovac, A. Voigt, P. Rasehman: J. Magn. Magn.Mater., 341 (2013) 93-99
9. R. Arulmurugan, G. Vidyanathan, S. Sendhinathan, B. Jeyadevan: Physica B Condensed Matter Phys., 363 (2005) 225
10. B. Zhou, Y. Zhang, C. Liao, C. Yan, L. Chen, S. Wang: Solid State Comm., 126 (2003) 593
11. S. K. Nath, K. H. Maria, S. Noor, S. S. Sikdar, S. M. Hoque, M. A. Hakim: J. Magn. Magn. Mater., 324 (13) (2012) 2116-2120
12. L. L. Hench, J. K. West: Principles of electronic Ceramics, Wiley, New York, 1990
13. P. Cousin, R. A. Ross: Mater. Sci. Eng. A, 130 (1990) 119-125
14. S. P. Dalwai, A. B. Gadkari, T. J. Shinde, P. N. Vasambekar: Adv. Mater. Lett., 4(7) (2013) 586-590
15. C. N. Rao: Chemical approaches to the synthesis of Inorganic Materials, Wiley Easter, New Age International, New Delhi, (1993)
16. A. Xia, C. Jim, D. du, Y. sun, L. Tang: J. Magn. Magn.Mater., 323 (2011) 2080-82
17. S. Ramesh, B. Chandra Sekhar, P. S. V. Subba Rao, B. Parvathewara Rao: Ceram. Int., 40 (2014) 8729-8735
18. Anjali Verma, Ratnamala Chatarjee: J. Magn. Magn.Mater., 306 (2006) 313-320
19. Q. Liu, J. h. Sun, H. R. Lang, X. Q. sun, X. j. Zhang, Z. Xu: Mater. Chem. & Phys., 108 (2008) 269-273
20. N.D. Chaudhari, R.C. Kambale, J.Y. Patil, S.R. Sawant, S.S. Suryavanshi: Materials Research Bull., Vol. 45 (2010) 1713 - 1719
21. Ch. Srinivas, B. V. Tirupanyam, A. Satish, V. Seshabai, D. L. Sastry, O. P. Caltun: J. Magn. Magn.Mater., 382 (2015) 15-19
22. Asghari Maqsood, M. Arshad: Physical & Computational Sci. (A), 55(2) (2018) 79-84
23. Manojit De., Aniruddha Mukharjee, H. S. Tiwari: Processing & Appl. Of Ceramics, 9(4) (2015) 193-198
24. R. Suresh, P. Moganavally, M. Deepa: IOSR Journal of Appl. Chem., 8(5) (2015) 01-05
25. B. H. Devmunde, A. V. Raut, S. D. Birajdar, S. J. Sukla, D. R. Shengule, K. M. Jadhav: J. of Nanoparticles, (2016) Article ID-4709687, 08 pages.
26. Kazi Haruum Maria, Shamima Choudhary, M.A.Hakim: International Nano. Letters, 3:42, (2013), 1-10
27. P. Ravindranathan, K. C. Patil: Am. Cerm. Soc. Bull., 66 (4) (1987) 688-92.
28. 28] R. G. Dorik, Kunal B. Modi and K. M. Jadhav., Ind. J. Pure and Appl. Phys. Vol. 35. (1997) 594-597.
29. J. L. Bhosale, S. N. Kulkarni, R. B. Sasmile, and B. K. Choughule., Bull. Mater. Sci. Vol. 19. No.5 (1996)767-774.
30. A. Hajalilou, M. Hashim, H. M. Kamari, M. T. Masoudi: J. of Nanoparticles, (2015) Article ID-615739, 11 pages.

31. F. Nakagomi, S.Da Silva, V.K.Garg, A.C.Oliveria, P.c.Morais, A.Jr. Franco: J.Solid State Chem., 182, (2009), 2423-2429
32. V.M.Khot, A.B.Solunkhe, M.R.hadature, N.D.Thorat, S.H.Pawar: J.Phys.D.Appl.Phys., 46, (2013) 055303, 1-8
33. Vara Prasad, B.B.V.S., Rajesh Babu, B., Siva Ram Prasad, M.: Material Science-Poland, DOI:10.1515/msp-2015-0111, (2015).
34. O. S. Josyulu and J. Sobhanandri, Phys.Stat Sol., (a) 65 (1981) 479.
35. R.D Waldron: Physical Review, 99(6), (1955) 1727-1735
36. S. Halfner, Z. Krist., 115 (1961) 331.
37. B. Evan, S. Hafner: J. Phys. Chem. Solids, 29 (1981) 1573
38. T. K. Pathak , J. J. U. Buch, U. N.Trivedi, H. H. Joshi, K.B. Modi: J. Nanoscience and Nanotechnology, 8 (2008) 4181-87
39. S. A. Mazen, H.M. Zaki, S.F. Mansour: Int. J. Pure and Applied Physics, 3(1), (2007) 40-48
40. W.A.Wooster: Rep. Prog. Phys., 19 (1953) 62
41. V.K.Lakhani, K.B.Modi: Solid State Sci., 12 (2010) 2134
42. V.Baldev Raj, P.Rajendran, Palanichamy: "*Science and Technology of Ultrasonics*", Narosa Pub. House, New Delhi, (2004), 250
43. A. Maqsood, M. Arshad: Phys. &Comput. Sci., 55 (2) (2018) 79-84
44. D.P.N. Hasselmann, R.M. Fulrath: J. Am. Ceram. Soc., 47, (1964), 52-53
45. O.L.Anderson: "*Physical Acoustics*",Vol. III, Part B, Acad. Press, NY, USA, (1965), 43
46. S. F. Pugh: Phil. Mag., 45, (1954), 823-843
47. E. Stern: J. Appl. Phys. 38, No. 3 (1967) 1397.
48. V. G. Panicker, R. V. Upadhyay, S. N. Rao, R. G. Kulkarni., Jour. Mater. Sci. Lett.3 (1984) pp-385-387.
49. B. R. Karche, B. V. Khasbardar, A. S. Vaingankar.,J. Magn. Magn. And Magn. Mater 168 (1997) pp-292-298